The Corrosion Behavior of Fe-Mn-Al Weld Metals

Daryush K. Aidun

(Submitted 31 August 2000; in revised form 10 October 2000)

The corrosion resistance of a newly developed iron-base, Fe-Mn-Al austenitic, and duplex weld metal has been examined in the NACE solution consisting of 5 wt.% NaCl, 0.5 wt.% acetic acid, and the balance distilled water. The electrochemical techniques such as potentiodynamic polarization, Tafel plots, linear polarization, cyclic polarization, and open-circuit potential versus time were employed. The Fe-Mn-Al weld metals did not passivate and exhibited high corrosion rates. Fe-Cr-Ni (310 and 316) weld and base metals were also examined in the NACE solution at room temperature. The 310 and 316 base metals were more resistant to corrosion than the as-welded 310 and 316 weld metals. Postweld heat treatment (PWHT) improved the corrosion performance of the Fe-Mn-Al weld metals. The corrosion resistance of Fe-Mn-Al weld metals after PWHT was still inferior to that of the 310 and 316 weld and base metals.

Keywords cylic polarization plot, Fe-Mn-Al weld metal, linear polarization plot, Tafel plot

1. Introduction

High-alloyed steels now are commonly used in oil fields and petroleum industry-related equipment. The environments encountered in these systems contain substantial amounts of hydrogen sulfide (H_2S), chloride ions ($C1^-$), and carbon dioxide (CO_2). The operating temperature ranges and the H_2S amounts increase with the excavation of deeper oil wells. These factors lead to a higher corrosion rate and cracking in the commercial materials typically used in these particular environments.

Chromium-nickel conventional stainless steels are used in oil and gas industry equipment,[1] mainly to resist cracking, which is widely encountered in the prescribed environment. The conventional stainless steels exhibit acceptable resistance to general corrosion attack and to localized corrosion such as pitting and crevice corrosion.

Fe-Mn-Al alloys are not yet used commercially. They are being tested to evaluate their performance and to compare them with other commercial alloys, such as the Cr-Ni austenitic stainless steels, because of their lower density and lower cost per pound. Studies of mechanical properties were conducted on Fe-Mn-Al base and weld metal alloys. Fe-Mn-Al weld metals were shown to possess better room-temperature mechanical properties than 310 and 316 weld metals.[2] In a stress-corrosion-cracking study,[3] in NACE solution, Fe-Mn-Al weld metals were more resistant to cracking than the conventional 310 and 316 stainless steel weld metals. However, the general corrosion behavior of the Fe-Mn-Al was inferior to that of the 310 and 316 weld metals.

Corrosion behavior, such as general attack and pitting corrosion of various heats of Fe-Mn-Al alloy, was investigated in chloride-bearing environments.[4–8] However, the corrosion behavior of Fe-Mn-Al weld metals in NACE solution has not been studied.

The aim of this study is to evaluate the general and pitting corrosion behavior of Fe-Mn-Al weld metals and to compare their performance with conventional 310 and 316 austenitic stainless steel weld metals. Commercial 310 and 316 stainless steel plates are also examined in the as-received condition for the purpose of comparison.

2. Experimental Procedures

The weld metal preparation was described previously.[2] The chemical composition, mechanical properties, and ferrite number contents of 310, 316, and Fe-Mn-Al weld metals (I through VI) are summarized in Tables 1 and 2, respectively. Samples extracted from each weld deposit (I, II, III, and V) were divided into two groups. The first group was mounted in an epoxy resin in the as-welded condition. The second group of samples was subjected to postweld heat treatment (PWHT) at 1090 ± 2 °C (1975 °F) for 40 min and then water quenched and mounted in the epoxy resin. Each mounted sample, including those of the base metals of 310 and 316, had an exposed area of approximately 1.5 × 2.5 cm. The side opposite to the exposed area inside the epoxy mount was attached to a conducting wire by nickel paste. The wire protruded from the mount side opposite to the exposed area and connected the sample to the working electrode cord coming from the potentiostat. Each exposed area was ground down to 600 grit, ultrasonically degreased in acetone, washed in distilled water, and dried in air prior to testing.

The corrosive medium and exposure procedures were as follows. NACE solution consisting of 5 wt.% NaCl, 0.5 wt.% acetic acid, and the balance distilled water was prepared. The samples were mounted on one side of the corrosion cell. The corrosion cell used in this study (flat cell by EG&G[9]) allowed a net area of 1 cm^2 to be exposed to the corrosion solution. It also provided a holding-fit assembly that minimized the crevice corrosion at the boundaries of the tested area. The NACE solution was added directly after the sample was mounted. Argon gas was then bubbled through the solution for 10 min, followed

Daryush K. Aidun, Department of Mechanical and Aeronautical Engineering, Clarkson University, Potsdam, NY 13699-5725. Contact e-mail: dka@clarkson.edu.

by H_2S gas bubbled for another 10 min. All polarization measurements started at the end of this stage. This procedure was followed to duplicate a similar procedure used in the stress-corrosion-cracking tests conducted on these weld metals.[3] The electrochemical tests included the potentiodynamic polarization, Tafel, linear polarization, cyclic polarization, and open-circuit potential versus time.

All tests were conducted at room temperature using an EG&G versastat potentiostat. A silver/silver chloride (Ag/AgCl) reference electrode was housed in a luggin well, which contained a fixed 1.5 mm OD Teflon® luggin capillary protruding from the bottom of the well. The luggin well was filled with NACE solution that flowed continuously in the luggin capillary from the well to the cell. The reference electrode was then inserted in the well. The luggin capillary was positioned at the center of the exposed area (working electrode), at a distance of approximately 1 mm from the surface of that area. The potentiostat has a built-in feature to compensate for the IR drop between the luggin capillary and the working electrode. Energy dispersive spectroscopy (EDS) was used in this study to determine the nature of the corrodent in the surface of the weld metals.

3. Results

Detailed solidification morphologies for the weld metals I through VI were reported previously.[2] Figure 1(a) and (b) show the typical solidification morphologies of weld metals I and 316, respectively. Ferrite-containing PWHT samples possessed different microstructural morphologies as well as different ferrite numbers (FNs). The PWHT weld metals I and III exhibited a microstructure containing a grid of square dark lines in a light matrix, instead of the dendritic morphology that they possessed in the as-welded condition (Fig. 1c). Table 2 summarizes the FNs and hardnesses (Vickers) of all weld metals, before and after PWHT. The FNs dropped to 0 from 7 and 6 for weld metals I and III, respectively. The PWHT weld metal II possessed a discontinuous dendritic structure and FN of 25. Weld metals V, 310, and 316 did not show much change in their solidification morphologies or in their FN contents. The hardness values of the PWHT samples were reduced compared to the values in the as-welded condition. The hardness values of the PWHT Fe-Mn-Al weld metals were 40 to 50 diamond pyramid hardness (DPH) lower than those of the as-welded metals.

Table 1 Chemical compositions of weld metals (wt%)

Weld metal	C	Si	Mn	Al	P	S	N	Fe
I	0.13	0.24	20.97	5.60	0.006	0.007	0.020	Bal
II	0.22	1.07	28.87	7.42	0.011	0.013	0.015	Bal
III	0.45	0.36	22.75	7.14	0.015	0.022	0.022	Bal
IV	0.98	1.40	31.07	10.73	0.028	0.007	0.007	Bal
V	0.50	0.20	20.00	5.00	0.005	0.005	0.020	Bal
VI	10.00	0.10	20.00	5.00	0.005	0.005	0.020	Bal

Weld metal	C	Si	Cr	Ni	Mn	Mo	P	S	N	Fe
310	0.1	0.45	26	21.0	1.8	0.0	0.024	0.007	0.045	Bal
316	0.1	0.40	19	12.5	1.8	2.3	0.012	0.013	0.023	Bal

4. Potentiodynamic Polarization Behavior

The potentiodynamic polarization curves of tested weld metals are shown in Fig. 2. Figure 2(a) shows the potentiodynamic curves of the as-welded and Fig. 2(b) shows the curves for PWHT weld metals. The starting values of the polarization scans were more active (more negative) by 250 mV than the corrosion potential (E_{corr}).

All Fe-Mn-Al samples, whether as-welded or PWHT, underwent active dissolution with no passivation observed on the anodic polarization side of the curves. The 310 and 316 weld metals (as-welded and PWHT), as well as the 310 and 316 plate samples, exhibited active-passive and transpassive features. The passive regions of the plate samples extended further than those of the stainless steel weld metal samples. In addition, the critical current density (i_{cc}) of the plate samples was less than that of the same weld metals.

5. Tafel Plots

A typical Tafel plot is shown in Fig. 3 for the cathodic and anodic polarization of weld metal III. The starting values of the Tafel plot measurements were more active by 250 mV, and

Table 2 Mechanical properties of the weld metals

Weld metal	YS(a)-ksi (MPa)(b)	TS-ksi (MPa)	El.(c) (%)(b)	DPH(b)	FN(b)	DPH(d)	FN(d)
I	61.0 (421)	98.5 (679)	47	203	7	156	0
II	81.0 (559)	113.0 (779)	15	271	52	221	25
III	70.5 (486)	107.0 (738)	50	240	6	193	0
V	74.0 (510)	109.0 (752)	49	253	0	201	0
310	69.5 (479)	85.5 (590)	12	268	0	257	0
316	64.5 (445)	96.5 (667)	33	272	0	247	0

(a) Yield strength at 0.2% offset
(b) As-welded
(c) Elongation in 1-in.-gage length
(d) PWHT

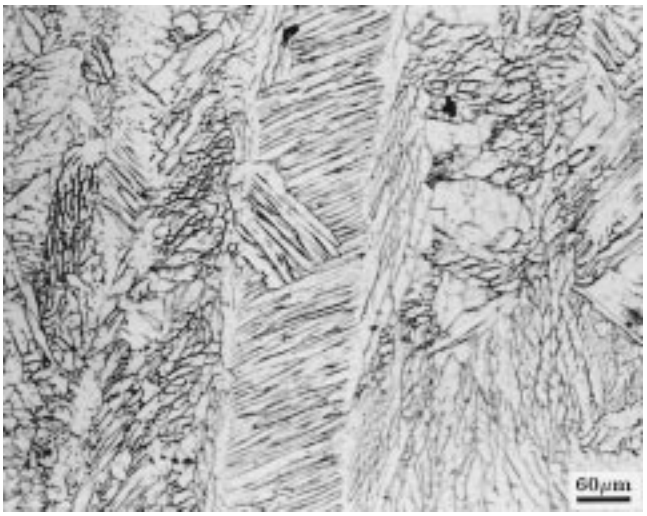

(**a**)

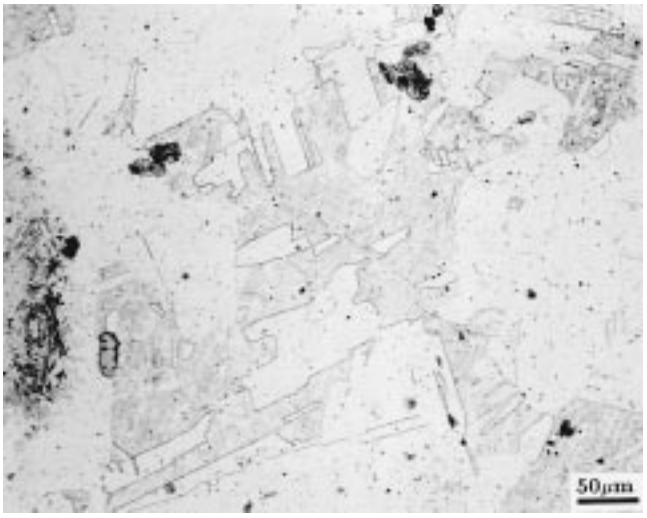

(**b**)

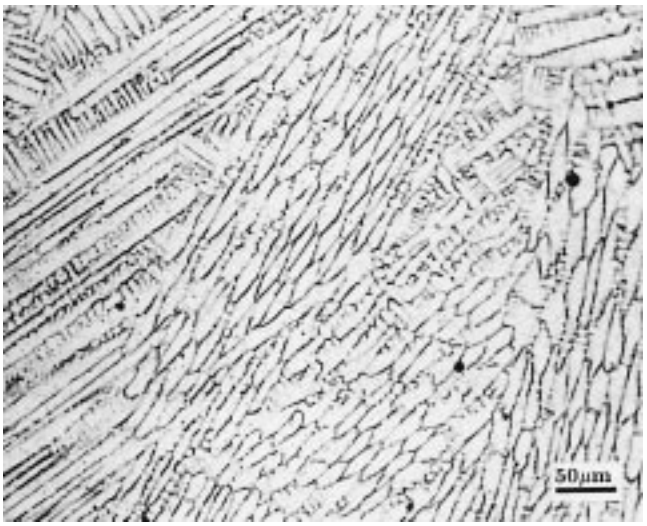

(**c**)

Fig. 1 Typical solidification morphology of (**a**) weld metal I in the as-welded condition, (**b**) weld metal I after PWHT, and (**c**) weld metal 316 in the as-welded condition

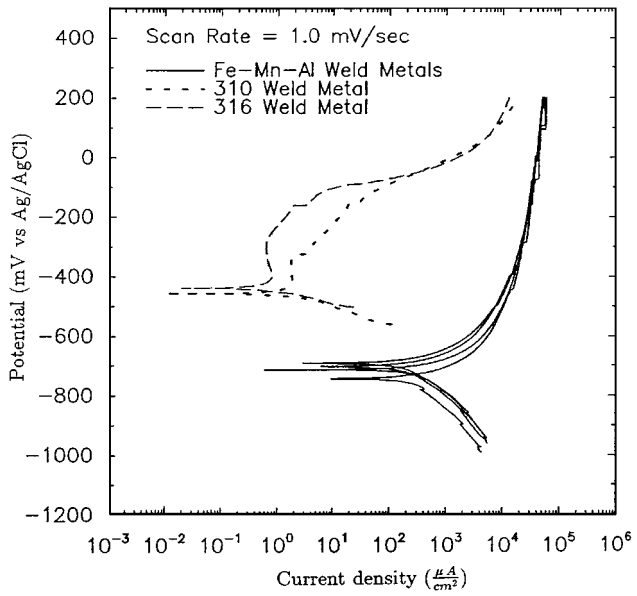

(**a**)

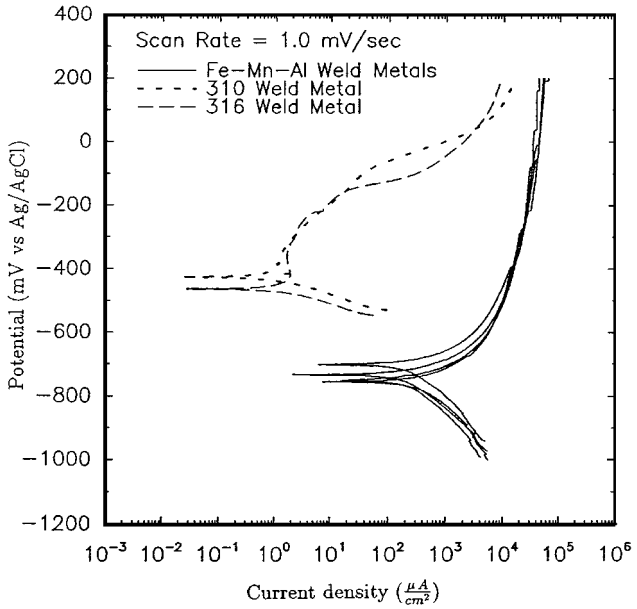

(**b**)

Fig. 2 Potentiodynamic curves of (**a**) weld metals in the as-welded condition and (**b**) weld metals after PWHT

the end values were more noble (more positive) by 250 mV than the E_{corr} with a scan rate of 0.2 mV/s.

The Fe-Mn-Al weld metals exhibited active behavior in the anodic part of the polarization curves. The Fe-Mn-Al was not as sensitive to scanning rates as concluded from the corrosion rate measurements conducted at both 0.2 and 1 mV/s. The corrosion rates in both cases were nearly equal. This may be due to the rapid and high corrosion tendency of Fe-Mn-Al weld metals resulting in the formation of a corrosion layer. The 310 and 316 weld metals showed active-passive and transpassive regions, as in the previous case.

Three Tafel polarization scans were performed to check the

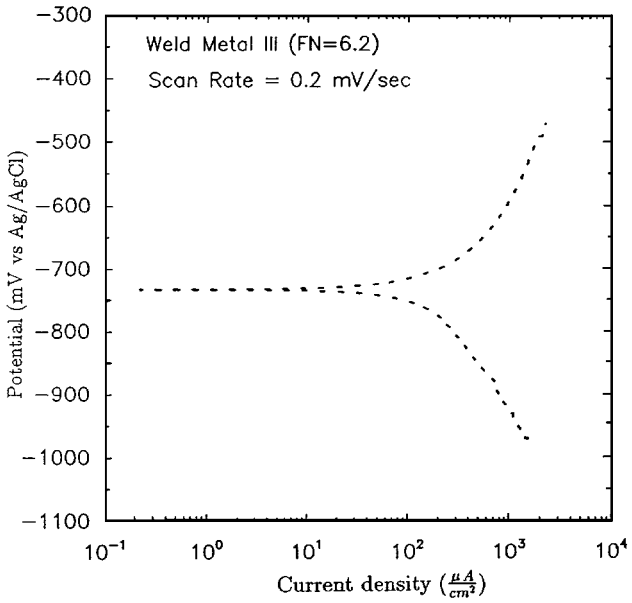

Fig. 3 Typical Tafel plot of weld metal III in the as-welded condition

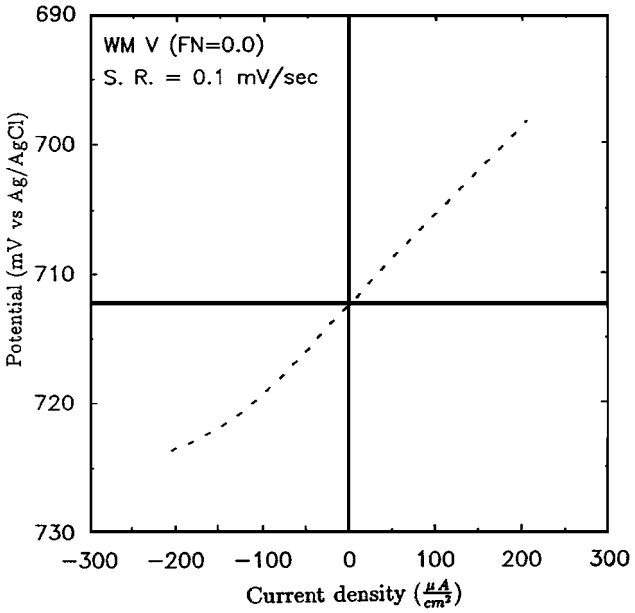

Fig. 4 Typical linear polarization curve of weld metal V after PWHT

Table 3 Corrosion data measured from Tafel analysis

Material	Condition	Corr. rate(a) mpy (mm/y)	Corr potential $mV_{Ag/AgCl}$
WM I	As-welded	86.5 ± 12.0% (2.2)	−742 ± 1.3%
WM I	Solution-annealed	77.0 ± 5.2% (2.0)	−739 ± 1.2%
WM II	As-welded	103.5 ± 14.3% (2.6)	−755 ± 1.8%
WM II	Solution-annealed	81.0 ± 0.7% (2.1)	−756 ± 1.1%
WM III	As-welded	85.5 ± 12.4% (2.2)	−742 ± 1.2%
WM III	Solution-annealed	77.0 ± 14.2% (2.0)	−732 ± 0.3%
WM V	As-welded	66.5 ± 1.6% (1.7)	−735 ± 1.0%
WM V	Solution-annealed	67.0 ± 11.1% (1.7)	−732 ± 0.5%
WM 310	As-welded	2.0 ± 9.1 (0.0)	−436 ± 4.7%
WM 310	Solution-annealed	0.8 ± 11.1% (0.0)	−414 ± 8.4%
WM 316	As-welded	0.5 ± 78.7% (0.0)	−404 ± 8.4%
WM 316	Solution-annealed	0.5 ± 32.6% (0.0)	−409 ± 3.7%
BM 310	As-received	1.4 ± 22.4% (0.0)	−376 ± 3.7%
BM 316	As-received	0.3 ± 92.5% (0.0)	−360 ± 116.9%

(a) Based on three (Tafel plot) tests

Table 4 Corrosion data measured form the linear polarization resistance

Material	Condition	Corr. rate(a) mpy (mm/y)	Corr. potential $mV_{Ag/AgCl}$
WM I	As-welded	69.4 (1.8)	−732
WM I	Solution-annealed	67.5 (1.7)	−731
WM II	As-welded	74.1 (1.9)	−742
WM II	Solution-annealed	71.0 (1.8)	−739
WM III	As-welded	67.8 (1.7)	−725
WM III	Solution-annealed	68.9 (1.8)	−717
WM V	As-welded	57.8 (1.5)	−716
WM V	Solution-annealed	55.9 (1.4)	−712
WM 310	As-welded	0.3 (0.0)	−392
WM 316	Solution-annealed	0.2 (0.0)	−378

(a) Based on one linear polarization resistance test

Table 5 Electrochemical pitting parameters for 310 and 316 materials

Material	Condition	E_b ($mV_{Ag/AgCl}$)	E_p ($mV_{Ag/AgCl}$)
WM 310	As-welded	−150	−285
WM 310	Solution-annealed	−145	−295
WM 316	As-welded	−90	−343
WM 316	Solution-annealed	−90	−333
BM 310	As-received	−120	−275
BM 316	As-received	−80	−270

reproducibility of the tests, and the average results are reported. The corrosion rate in both mils per year (mpy) and milimeters per year (mm/y) and the corrosion potential (E_{corr}) for all tested samples are shown in Table 3. The maximum corrosion rate was exhibited by the as-welded weld metal II (FN = 52). Weld metals I and III exhibited nearly the same corrosion rate in both the as-welded and PWHT conditions. Weld metal V (FN = 0) exhibited the lowest corrosion rate among all the Fe-Mn-Al weld metals tested in the as-welded condition.

6. Linear Polarization

Instantaneous corrosion rates can be determined using the linear polarization or polarization resistance technique.[10] This technique was used to measure the corrosion rates and to compare them with the corrosion rates computed from the Tafel analysis. The linear polarization technique generally yields corrosion rates differing by no more than a factor of 3 from the actual corrosion rates.[11] The polarization plots were constructed for all tested samples at a scan rate of 0.1 mV/s. Fig.

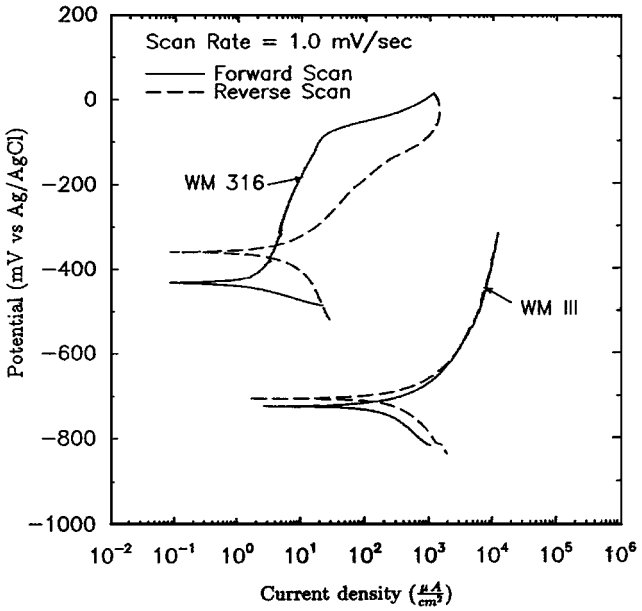

Fig. 5 Typical cyclic polarization curves of weld metals III and 316 in the as-welded condition

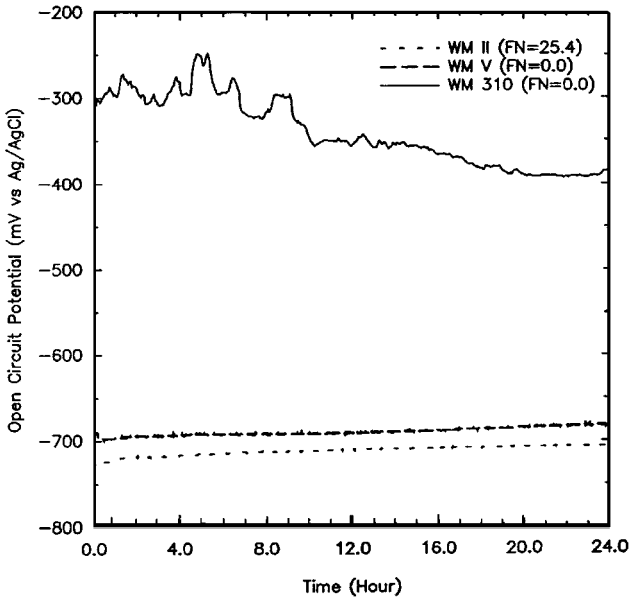

Fig. 6 Typical open-circuit potential vs time of weld metals II, V, and 310 after PWHT

4 shows a linear polarization plot for weld metal V. The corrosion rates computed using this technique are shown in Table 4. The corrosion rates computed from the linear polarization technique were in good agreement with the corrosion rates computed from the Tafel analysis. The corrosion rates in Table 3 and 4 should be used only for comparison purposes.

7. Cyclic Polarization

The cyclic polarization technique was used to evaluate the pitting behavior of the two weld metal systems. This technique involves a controlled-potential forward scan starting from a potential usually equal to or less than E_{corr}, up to a potential higher than the breakdown potential (E_b). The breakdown potential is a potential at which the permanent onset of localized corrosion (pitting) takes place. The point at which the forward scan ends and the reverse scan starts in specified by ASTM G61[12] as the point at which the current reaches 5 mA. In this study, this point was taken at a potential that was more noble by 400 mV than E_{corr} (Fig. 5). The important result obtained from the cyclic polarization curves was that none of the Fe-Mn-Al weld metals exhibited a distinctive hysteresis loop, while the cyclic polarization curves of the 310 and 316 samples all possessed a hysteresis loop.

The cyclic polarization curves corresponding to the stainless steel samples (310 and 316) were used to obtain two terms: breakdown potential (E_b) and protection potential (E_p). The E_p was determined at the point at which the reversed scan curve intersected the forward scan curve. The different values of E_b and E_p of the stainless steel samples are shown in Table 5.

8. Open-Circuit Potential versus Time

Studies of a freely corroding material without polarization describe how the material reacts with its environment. This technique shows the stability of the material in a specific corrosion medium and whether it will equilibrate or undergo a continuous reaction. The open circuit potential (E_o) versus time was recorded for all samples up to 24 h of exposure. During exposure, E_o was recorded every 60 s during the entire duration (Fig. 6)

The open-circuit potential of the Fe-Mn-Al weld metals shifted to the more active direction at the beginning of the exposure during the first hour. The E_o then started a slow stable shift in the noble direction and reached potentials more noble than the E_{corr} reported in Table 3. The same behavior was exhibited by both the as-welded and solution-annealed Fe-Mn-Al weld metals. However, the final open-circuit potential of the solution-annealed samples was relatively more noble than that of the as-welded Fe-Mn-Al samples.

The Fe-Cr-Ni samples exhibited a different behavior. Immediately after exposure, the open-circuit potential shifted in the active direction and then started a complex behavior of perturbations. The Fe-Cr-Ni samples, whether as-welded, solution-annealed, or as-received, did not stabilize during the 24 h exposure duration. They all showed an unsystematic behavior of shifts from the active to the noble direction or *vise versa*. This indicates that passive-film disruption and repair processes take place during exposure to the corrosion medium.

9. Discussion

Clearly, the Fe-Mn-Al weld metals are inferior to the conventional 310 and 316 weld and base metals. The corrosion potentials of the Fe-Mn-Al were more active by at least 300 mV than the corrosion potentials of the 310 and 316 stainless steels (Tables 3 and 4). Corrosion rates exhibited by the Fe-Mn-Al were unacceptable and cannot be compared to those exhibited by the Fe-Cr-Ni weld and base metals (Tables 3 and 4). The

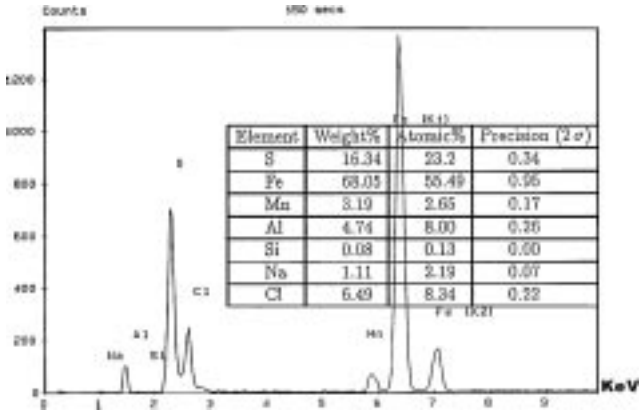

Fig. 7 EDS analysis of corrosion film on weld metal II (in the as-welded condition)

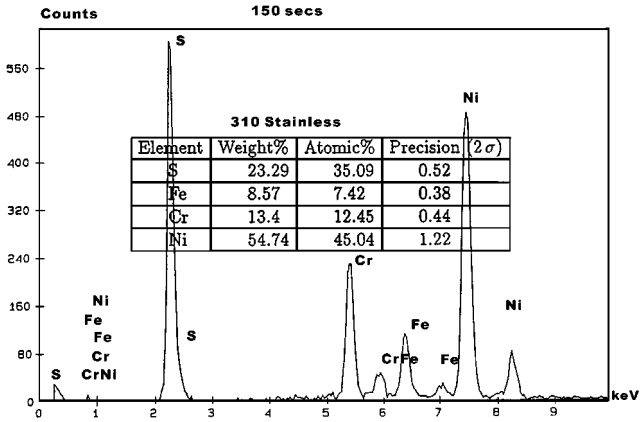

Fig. 8 EDS analysis of a small, corroded area on 310 as-welded sample

pitting resistance of the Fe-Mn-Al weld metals may appear to be better than that of the 310 and 316 stainless steels, as shown in Fig. 5. The absence of real hysteresis loops for the Fe-Mn-Al samples is due to the formation of a corrosion film that totally covered the material's exposed surface. However, an active type of corrosion can also occur when the corrosion rate is large but without a corrosion product layer formed. Energy dispersive spectroscopy (EDS) analysis of WM II revealed that this corrosion film is composed mainly of iron, sulfur, and chloride components (Fig. 7). Upon reversing the potentials, the reversed curves nearly overlapped the forward scanned curves, with no indication of any repassivation process that was clear in the case of the 310 and 316 samples (Fig. 5).

The PWHT improved the performance of the Fe-Mn-Al weld metals; however, even with the improvement, the corrosion rates are still higher than any acceptable level. The improvement can be attributed to FN reduction due to heat-induced ferrite dissolution. The ferrite has a detrimental effect on the general corrosion behavior. Table 3 shows higher corrosion rates for the ferrite-bearing weld metals. It is important to note that the fully austenitic (FN = 0) weld metals, *i.e.*, weld metal V before PWHT and weld metals I, III, and V after PWHT, all possessed nearly the same corrosion rates, as shown in Table 3. It is suggested that this "relative" improvement is due to the enhanced distribution of aluminum (the major element that aids the corrosion resistance in this alloy system) in the austenitic matrix. Before the PWHT, an aluminum concentration gradient existed between the ferrite and the austenite. The PWHT resulted in a ferrite to austenite transformation and reduced or eliminated the concentration gradient, such as in the case of weld metal II and weld metals I and III, respectively.

The poor performance of the Fe-Mn-Al weld metals in this corrosive medium can be attributed to a number of factors. The presence of H_2S is very detrimental and has a negative effect on the stability of the passive film.[13] It promotes general and localized corrosion such as pitting and stress corrosion cracking. Also, the addition of H_2S to an aqueous solution tends to lower the pH values. Chloride ions that exist in NACE solution have a well-known role in aiding the corrosion problem in general and pitting corrosion in particular. All these factors led to the severe general corrosion attack experienced by all of the Fe-Mn-Al weld metals.

Different results were obtained for the 310 and 316 weld and base metals in the as-received, as-welded, and PWHT conditions. The as-received base metals of 310 and 316 stainless steel plates performed better than the as-welded 310 and 316 weld metals. The plates possessed a lower i_{cc} and more noble E_b, E_p, and E_{corr}. Although the discrepancies between the stainless steel weld and base metals are not great, they show that the weld metals are indeed more susceptible to corrosion than the base metals. This susceptibility occurs because the weld metal system is heterogeneous, due mainly to the fast cooling rates involved in the welding process, which result in segregation and uneven distribution of the alloying elements.[14] In the case of the fully austenitic (FN = 0) stainless steel weld metal tested in this work, carbides may have formed, thus depleting the Cr in the austenitic matrix (sensitization). Another factor that may have contributed to the chromium depletion is the formation of the σ phase.[15] The comparison of the as-welded and the PWHT stainless steel weld metals supports the theory of Cr depletion. The PWHT at 1090 ± 2 °C (1975 °F), followed by the water quench process, helped to return Cr to the austenitic matrix and improved the corrosion properties of the weld metals. The E_b is more noble in all 316 weld metals, while the E_p is more noble in the 310 as-welded and PWHT weld metals (Table 5). The E_b is more noble in 316 due to the presence of Mo in these materials. Molybdenum has been reported[16] to be beneficial to the pitting resistance of austenitic stainless steel alloys. The EDS analysis conducted on a small, corroded area of a 310 as-weld sample is shown in Fig. 8. The profile shows high contents of S, Ni, and Cr components in the corrosion products.

It is well established that chromium is responsible for the corrosion resistance in the conventional stainless steels. It is also known that aluminum is responsible for the corrosion resistance in the Fe-Mn-Al alloy system. However, this study shows that Al cannot replace Cr in providing adequate corrosion resistance to a ternary iron-base alloy system, at least in this particular corrosive environment (NACE solution). This conclusion is similar to the observations of Altsletter *et al.*,[6] who compared the corrosion performance of Fe-Mn-Al alloys to Cr-alloyed steels in different corrosion environments.

10. Conclusions

This study was conducted to examine and compare the corrosion performance (in NACE solution) of Fe-Mn-Al and Fe-Cr-Ni weld metals. The main conclusions are as follows.

- The Fe-Mn-Al weld metals exhibited unacceptable corrosion rates, while the Fe-Cr-Ni weld and base metals possessed excellent corrosion resistance.
- Postweld heat treatment improved the corrosion performance of Fe-Mn-Al weld metals by decreasing the ferrite content. Ferrite was found to have a detrimental effect on the corrosion resistance of Fe-Mn-Al weld metals. However, the enhancement achieved by PWHT with the Fe-Mn-Al weld metals did not reduce the corrosion rates to an acceptable level.
- The 301 and 316 base metals performed better than the as-welded 310 and 316 weld metals.

References

1. *Metals Handbook*, 10th ed., vol. 1, *Properties and Selection: Irons, Steels, and High Performance Alloys*, ASM International, Metals Park, OH, 1990, p. 879.
2. K. Makhamreh and D.K. Aidun: *Welding J.*, 1992, Mar., pp. 104s-113s.
3. K. Makhamreh and D.K. Aidun: *Welding J.*, 1993, June, pp. 247s-255s.
4. V.P. Batrakov *et al.*: *Prot. Met.*, 1974, vol. 10, p. 487 (English translation).
5. R. Wang and F.H. Beck: *Met. Progr.*, 1983, vol. 123, p. 73.
6. C.J. Altstetter, A.P. Bentley, J.W. Fourie, and A.N. Kirkbride: *Mater. Sci. Eng.*, 1986, vol. 82, p. 13.
7. W.T. Tsai, J.B. Duh, and J.T. Lee: *J. Mater. Sci.*, 1987, vol. 22, p. 3517.
8. J.B. Duh, W.T. Tsai, and J.T. Lee: *Corrosion*, 1988, vol. 44, p. 810.
9. EG&G, Princeton Applied Research, Gaithersburg, MD, Publication No. 220690-A-MNL-A, 1989.
10. R.J. Jasinski and K.D. Efird: *Corrosion*, 1987, vol. 43, p. 476.
11. M.G. Fontana: *Corrosion Engineering*, 3rd ed., McGraw-Hill, New York, NY, 1986, p. 502.
12. "Standard Test Method for Conducting Cyclic Potentiodynamic Polarization Measurents for Localized Corrosion Susceptability of Iron-, Nickel-, or Cobalt-Based Alloys," ASTM G 61-86, *Annual Books of ASTM Standards 03.01*, ASTM, Philadephia, PA, 1987, p. 225.
13. Y. Yoshino and A. Ikegaya: *Corr. Sci.*, 1985, vol. 41, p. 105.
14. *Welding Handbook*, 7th ed., vol. 1, *Fundamentals of Welding*, American Welding Society, Miami, FL, 1981, p. 124.
15. A. Garne: *Mater. Performance*, 1982, p. 9.
16. F. Robinson and P. Biljon: *Corrosion*, 1985, vol. 41, p. 220.